Digest Journal of Nanomaterials and Biostructures Vol. 15, No. 2, April - June 2020, p. 367 - 374

STRUCTURAL AND ELECTRICAL PERFORMANCE OF MoO_3/Li/MoO_3 FILMS DESIGNED AS MICROWAVE RESONATORS

S. E. AL GARNI[a], A. F. QASRAWI [b,c,*], S. R. ALHARBI[a]
[a]*Department of Physics, Faculty of Science, University of Jeddah, Jeddah, Saudi Arabia*
[b]*Department of Physics, Arab American University, Jenin, Palestine*
[c]*Group of physics, Faculty of Engineering, Atilim University, 06836 Ankara, Turkey*

In this work, the effect of the insertion of lithium slabs of thicknesses of 50 nm between stacked layers of MoO_3 is considered. Stacked layers of MoO_3 comprising lithium slabs are prepared by the thermal evaporation technique onto Au substrates under vacuum pressure of 10^{-5} mbar. The effects of Li slabs are explored by the X-ray diffraction, scanning electron microscopy, current-voltage characteristics and impedance spectroscopy techniques in the frequency domain of 0.01-1.80 GHz. While the presence of Li slabs did not alter the amorphous nature of structure, it forced the growth of rod-like grains of diameters of 100-160 nm and lengths of 1.5 μm. Electrically, the presence of Li in the samples enhanced the rectifying properties of the devices and force reverse to forward current ratios larger than 60 times. Li slabs also controlled the negative capacitance effect and resonance –antiresonance regions in the Au/MoO_3/MoO_3/C stacked layers. While the Au/MoO_3/MoO_3/C devices displayed high conductance and low impedance values in the studied frequency domain, the Au/MoO_3/Li/MOO_3/C devices exhibited low conductance and high impedance mode in the frequency domain of 0.01-0.59 GHz. It is also found that the presence of Li slabs improved the performance of the devices through driving it to exhibit lower reflection coefficient and high return loss values near 0.80 GHz. The features of the devices nominate them for use as RF-Microwave traps or resonators.

(Received January 19, 2020; Accepted April 17, 2020)

Keywords: Au/MoO3/Li/MoO_3/C, X-ray diffraction, Negative capacitance, Return loss factor

1. Introduction

Stacked layers of molybdenum trioxide are employed in many technological applications to enhance the optoelectronic devices performances. In a recent work, the MoO3/Au/MoO3 electrodes which are fabricated by the mild thermal evaporation technique, succeed in enhancing the efficiency of four- terminal perovskite/silicon tandem solar cells up to 27% [1]. Au/MoO_3 interfaces are also reported to be suitable as ultraviolet photodetectors [2]. These interfaces displayed a high responsivity of ~ 0.5 A/W, a fast response time under UV-light (360 nm) irradiation and a photo/dark current ratio of over 6 nominating the Au/MoO_3 interfaces for efficient UV-light detection. In addition, Au/MoO_3/Au devices are mentioned to exhibit hysteresis and negative differential resistance (NDR) under time-varying voltage [3]. The device which was tested at 55–80 °C was nominated as memory devices.

In another work, nanoribbons of molybdenum trioxide are employed to enhance the conductivity and polarity of two dimensional materials for the purpose of improving their performance as the host for sulfur cathode in lithium–sulfur batteries [4]. The participation of MoO_3 nano ribbons forced better electrochemical performance as sulfur hosts with better rates and cycle performance. These batteries delivered an initial specific capacity of 1390.3 mAh/g at 0.1 C with the Coulombic efficiency of 99.7%. The retention of the initial capacity over 500 cycles at 1

* Corresponding author: atef.qasrawi@aaup.edu

C reached 79.6%. In addition, in another efficient work [5], the presence of MoO_3 as positive electrode in Li-S batteries enabled the Li-S battery to reveal an initial capacity of 1145 mAh/g and a retention capacity of 976 mAh/g after 1000 cycles. The coulombic efficiency for these batteries reached 99.54% at 1 C.

From optics point of view, the insertion of Li nano-slabs between stacked layers of MoO_3, enhanced the light absorbability by 11.0 times at 2.0 eV [6]. It also engineered the energy bands gap of molybdenum oxide in the range of 3.05–0.45 eV. Li was also able to convert the conductivity type of MoO_3 from *n*- to *p*-type, increases the drift mobility and also engineered the plasmon frequency in the range of 0.32–5.94 GHz. The novelty of the presence of Au, Li and MoO_3 at a time in the same device which is observed from the above mentioned discussion, motivated us to study the structural, morphological and electrical performance of the Au/MoO_3/Li/MoO_3/C devices. The stacked layers of molybdenum trioxide which are coated onto Au substrates are sandwiched with Li slabs of thicknesses of 50 nm. Herein we will compare the performance of the devices in the presence and the absence of Li slabs. Particularly, the crystalline nature, the current-voltage characteristics, the capacitance, the conductance, the impedance, the magnitude of the reflection coefficient and the return loss spectra will be studied in the frequency domain of 0.01-1.80 GHz. The study will allow exploring the nature of ac conduction mechanisms and classify the possible electronic applications of the devices. The role of Li slabs will be accounted on each of these parameters.

2. Experimental details

Stacked layers of MoO_3 thin films are grown onto Au substrates by the physical evaporation technique under vacuum pressure of 10^{-5} mbar using VCM-600 thermal evaporator. The source material is high purity (99.999%) MoO_3 nano-powders (Alfa-Aeser). The first layer was 500 nm thick. This layer is coated with Li (99.99% Alfa Aeser) nanosheets of thicknesses of 50 nm. The resulting MoO_3/Li films are covered with another MoO_3 layer of thickness of 500 nm. The films thicknesses were determined with the help of an INFICON STM-2 thickness monitor attached to the evaporator. Point carbon contacts of area of $3.14 \times 10^{-2}\ cm^{-2}$ were located on the top layer of MoO_3. The fabricated thin films are studied by means of X-ray diffraction (XRD) technique using Miniflex 600 XRD unit, scanning electron microscopy using COXEM 200 microscope and by Keithley current-voltage characteristics system equipped with 235-voltage source and 6485 Pico ammeter. The impedance spectroscopy is recorded in the frequency range of 0.01–1.8 GHz using Agilent 4291B 1.0M–1.8 GHz impedance analyzer. The connections to the fixture (16453A dielectric material test fixture) were made by AP-7 connector attached to the analyzer.

3. Results and discussion

To be able observe the effect of the lithium nano-slabs on the structural and electrical properties of molybdenum oxide which are coated onto Au substrates we will also consider the properties of two stacked layers of MoO_3 in the absence of lithium nano-slabs (MLM-0). The geometrical design for the Au/MoO_3/Li/MoO_3/C (MLM-50) samples are shown in inset-1 of Fig.1. The thickness of the lithium layer is 50 nm. Fig. 1 shows the X-ray diffraction (XRD) patterns for the studied samples. The figure display sharp peaks that are related to the Au substrates (JCPDS card no. 01-1172). The apparent sharp peaks indicate that the Au substrate is highly oriented along the (111) reflection direction. One intensive peak which appears at $2\theta = 35.1^{o}$ is assigned to orthorhombic Au_2O_3 [7]. No other intensive reflection peaks were found in the figure. The XRD patterns illustrate the amorphous nature of the grown Au/MLM-0 and Au/MLM-50 films owing to the observatory of no sharp peaks in the figure. This result is consistent with the early published data for glass/MLM samples comprising 50 nm Li but coated onto glass substrates [6]. The lithium induced crystallization process in MoO_3 was previously observed for stacked

layers of molybdenum oxide which contains Li slabs of thicknesses of 100 and 200 nm. The induced crystallization for sufficiently thick slabs of Li between layers of MoO_3 was ascribed to ionic substitutions of Li^{+3} in sites of Mo^{+6} which motivates formation of Li_2O bonds at the ultrathin interface between Li and MoO_3 [6].

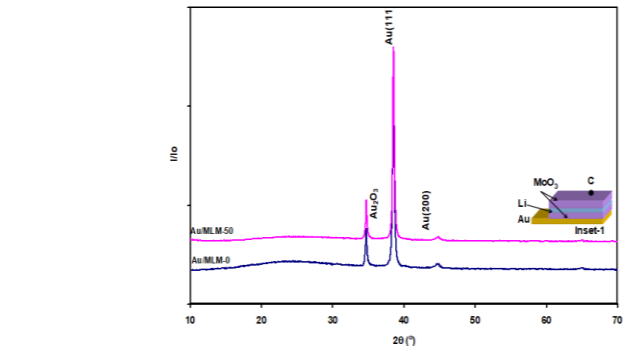

a)

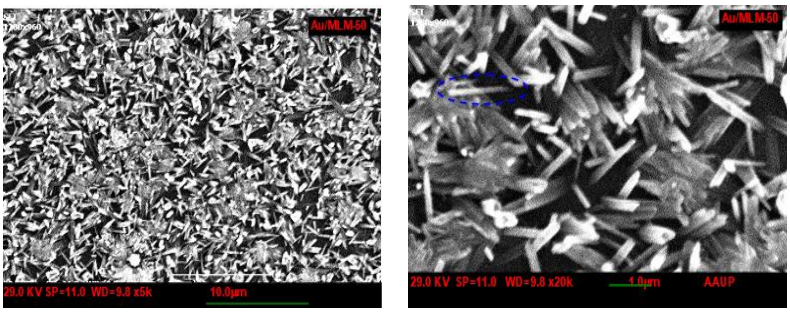

b)

Fig.1. (a) The X-ray diffraction patterns for stacked layers of MoO_3 grown onto Au substrates before and after the insertion of lithium slabs of thicknesses of 50 nm.
Inset-1 of (a) shows the geometrical design.
(b) Scanning electron microscopy images for the Au/MoO_3/Li/MoO_3 samples being enlarged 5000 and 20000 times.

On the other hand, inset-2 of Fig. 1 show the scanning electron microscopy images for an enlargement of 5000 times for the Au/MLM-50 samples. No image was recordable for the Au/MLM-0 samples. It is clear from the inset that the Au/MLM-50 samples are composed of very crowded, randomly distributed needle like grains. Further enlargement up to 20000 times (illustrated in inset-3 of Fig.1) allowed observatories of the needles like accumulations. Inset-2 of Fig.1 displays straight rods of average lengths of 1500 nm and diameter of 160 nm. Other rods (shown by dashed blue circle in the inset) reached length of 1600 nm and diameter of 100 nm. These preferred grain shapes were achieved via insertion of Li slabs between the stacked layers of the films. Formation of a rod like grains of lengths of 1.0-2.0 μm in lithium -aluminum silicate (LAS) glasses nucleated by P_2O_5 was ascribed to the lower nucleant density that allows grains to grow before impingement on one another [8]. We believe that the presence of lithium on the top of the first layer of MoO_3 strongly lowered the density the nucleons during the compensation of the second layer allowing the grains to grow separately before accumulation in groups.

The current (I)-voltage (V) characteristics for the Au/MLM-0/C and Au/MLM-50/C devices are illustrated in Fig. 2 (a) and (b), respectively. It is clear from Fig. 2 (a) that the $I-V$ variations follow approximately linear relationship. The ratio between the reverse (I_R) and forward (I_F) currents ($R_I = \frac{I_R}{I_F}$) at particular applied voltage is low. As for examples, at an applied voltage value of 0.40 V, the reverse to the forward current ratio is only 1.56. This value indicates that the Au/MLM-0/C device mostly behaves as a resistor rather than Schottky barrier. On the other hand,

the stacked layers of MoO_3 which comprises lithium slabs of thickness of 50 nm exhibits tunneling diode features presented by larger reverse currents values. The $I-V$ characteristics for the Au/MLM-50/C devices which is illustrated in Fig. 2 (b) display large difference between forward and reverse current values. As shown in Fig. 2 (c), the current ratio, R_I, increases with increasing biasing voltage. The $R_I - V$ variation follows two trends of variation. Namely, it sharply increases with increasing basing voltage reaching a value of 52.6 at 4.0 V and then tends to follow slower slopes in the remaining range of voltage biasing (4.0-8.0 V). The maximum obtainable R_I value is 69.1 at 8.0 V.

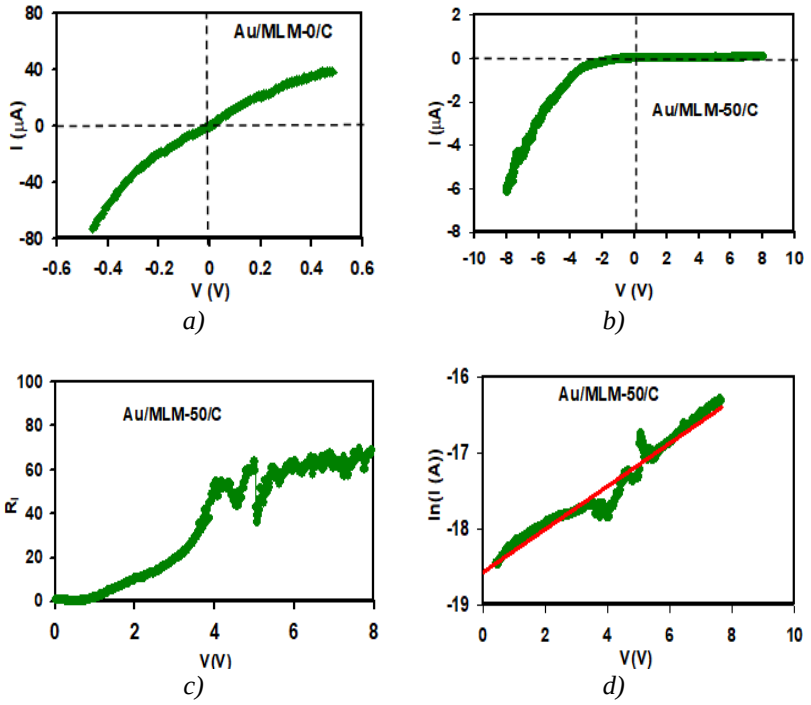

Fig. 2. The current voltage characteristics for (a) Au/MLM-0/C and (b) for Au/MLM-50/C devices. (c) The biasing voltage dependence of the reverse to forward current ratios and (d) the $Ln(I)-V$ variation under forward basing conditions.

Getting benefit from the linearity of the $\ln(I)-V$ characteristics of the forward (shown in Fig. 2 (d)) and reverse $\ln(I)-V$ curves which were carried out at $T = 300\,K$ assuming the validity of Richardson-Schottky equation, $I = AA{**}\,T^2 e^{-\frac{q\phi}{kT}}(e^{\frac{qV}{kT}}-1)$ [9] for a diode of area of A =3.14 $\times 10^{-2}\ cm^{-2}$ and Richardson constant ($A^{**} = 120m^*, (m^*_{MLM-50} = 0.409m_o$ [6])) constant value of 49.1 A/cm^2K^2 reveal barrier height ($q\phi$) value of 0.75 and 0.72 eV for forward and reverse biased devices, respectively. The lower barrier height at the Au/MLM-50 interface compared to the C/MLM-50 is one reason for the higher current values during reverse biasing process.

For the Au/MLM-0/C devices, it is also noticeable that the current values at any particular applied voltage are high when compared to the values obtained from the Au/MLM-50/C device (Fig. 2 (b)). The presence of Li nano-slabs between layers of MoO_3 remarkably decreased the current values and forced the device to behave like passive mode devices. While low values of basing voltage ($V = 0.40\,V$) were sufficient to achieve a current of 32.9 μA in the Au/MLM-0/C devices, the same current cannot be achieved even at 8.0 V in the Au/MLM-50/C devices. The numerical data suggests that the presence of lithium between layers of MoO_3 has altered the bonding mechanisms and/or formed specific interactions at the ultrathin interface region between Li and MoO_3. In our earlier study on the same samples, we have shown that for the stacked layers of MoO_3 which comprises Li slabs of thicknesses of 100 nm [6], Li_2O thin layers are formed at the

ultrathin interface. The peaks of the Li_2O appeared in the X-ray diffraction patterns of MoO_3 films. The exchange in the bonding mechanisms between Mo-O and Li-O should be the main reason for the drastically droping current values and it is also a reason for the enhancement in the rectifying properties of the Au/MLM-0/C devices. It is also worth reminding that the presence of Li leads to the formation of a rod like grains that are (as appears in the insets of Fig.1) randomly distributed. This leads to wider grain boundaries that in turn increases the resistivity of the material and make the current transport harder [10, 11].

The effect of Li slabs insertion between layers of MoO_3 on the alternating current conduction is evident from the capacitance (C) and conductance (G) spectra which are presented in Fig. 3 (a) and (b), respectively. Both physical parameters were measured at exciting voltage of 0.10 V in the frequency domain of 0.01-1.80 GHz. While the capacitance spectra of the Au/MLM-0/C samples display negative capacitance (NC) effect in the frequency domain of 0.01-0.82 GHz and 1.45-1.80 GHz, the Au/MLM-50/C samples display negative capacitance effect in a narrower region of 0.62-0.80 GHz. Except for the behavior of C in the 0.62-0.80 GHz region, $C-$spectra displays positive values in the studied range of frequency. The negative capacitance effect is beneficial for parasitic capacitance cancellation and noise reduction. It is also observed from Fig. 3 (a) that while the $C-$spectra of Au/MLM-0/C samples display resonance at 1.45 GHz followed by anti-resonance at 1.48 GHz and an antiresonance peak at 0.80 GHz, the Au/MLM-50/C samples display resonance and antiresonance at 0.61 and 0.62 GHz, respectively, and another antiresonance peak at 0.80 GHz. Such resonating peaks nominate the devices for use as microwave resonators. The negative capacitance effect was previously observed for Au/ZnSe/In/ZnSe/C interfaces [12]. Stacked layers of ZnSe comprising indium slabs of 75 nm thicknesses (ZIZ) displayed NC effect in the frequency domain of 0.01-1.80 GHz. This behavior was ascribed to surface charge flowing from the ZIZ to the Au or carbon metals. It is mentioned that, the connection allows flowing of minority carriers to one of the Schottky devices while the other side is forward biased (subjected to majority carrier flow). NC effect accompanied with resonance-antiresonance phenomena was also observed in $Au/Bi_2O_3/ZnS/Ag$ [13] devices and was attributed to presence of more than one stacked layer in the device. It is reported that while one stacked layer is at resonance, the other set all its charge carriers free due to the inability of the dipole to follow the signal causing the antiresonance case.

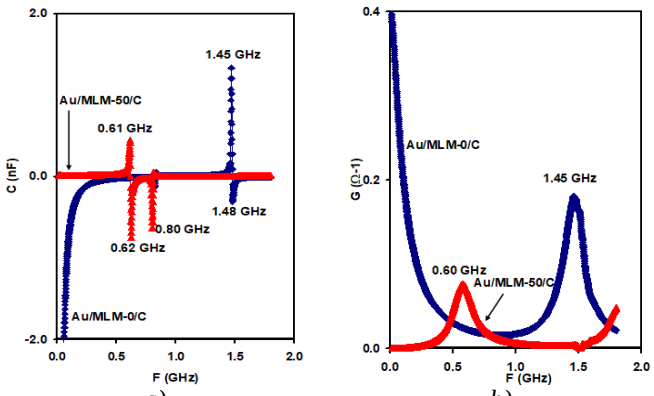

Fig. 3. (a) the capacitance and (b) the conductance spectra for stacked layers of MoO3 coated onto Au substrates before and after the insertion of Li slabs.

On the other hand, the conductance spectra which appear in Fig. 3 (b) display characteristics that seems to be highly influenced by the lithium layers. Particularly, while the $G-$ spectra of the Au/MLM-0/C devices display a sharp decrease in the values of G with increasing frequency from 0.39 Ω^{-1} at 0.01 GHz to 0.011 Ω^{-1} at 0.88 GHz, the Au/MLM-50/C devices display an increasing trend of variation in the frequency domain of 0.01-0.60 GHz. The conductance spectra of the Au/MLM-0/C sample display maximum peaks at 1.45 GHz. This peak shifts to 0.60 GHz upon Li insertion in the structure of MoO_3. This shift is accompanied with

decrease in the value of the maximum conductance at peaks centers. Earlier studies of similar device structures ascribed this behavior of $G-F$ response to changes in the current conduction mechanisms. Namely, the peak in the G- spectra is believed to arise from the changes in the controlling parameters of the current conduction mechanism [14, 15]. The domination of quantum mechanical tunneling (QMT) or correlated barriers hopping (CBH) always depends on the density of localized states near the Fermi level ($N(E_F)$). It is mentioned that for CuO at particular temperature, the density of localized states near the Fermi level decreases with increasing ac signals frequency. Since the conductivity is proportional to the square of $N(E_F)$, any decrease in $N(E_F)$ will necessarily decrease the value of conductivity or conductance [14, 15]. The peak appears at the turning point where the current conduction convert from CBH to QMT or from QMT to CBH. Diffusion of Li into the structure of MoO_3 to form Li_2O [6, 12] significantly alters the number of vacant sites in MoO_3 leading to a decrease in the number of traps or defects and as a result a decrease in the values of $N(E_F)$ should take place.

From practical point of view, there is a need to determine the impedance (Z) spectra of the proposed devices. The impedance is calculated from the relation, $=\sqrt{G^{-2}+(wL-(wC)^{-1})^2}$, with L being the measured inductance at an angular frequency w [16]. The impedance spectra are shown in Fig. 4 (a). It is clear from the figure, that the insertion of the Li nano-slabs between layers of MoO_3 has significantly altered the dynamics of the impedance spectra. Namely, while the Au/MLM-0/C samples show low values of impedance, the impedance of Au/MLM-50/C samples display much larger value. Z values increases with increasing signal frequency in the samples not comprising Li slabs and decreases with increasing signal frequency in the presence of Li slabs. As for examples, while the impedance values of the Au/MLM-0/C increase from 0.7Ω to 72.5 Ω (center of maximum peak) in the frequency domain of 0.01-0.84 GHz, Z values of Au/MLM-50/C devices decreases from 874 Ω to 13 Ω as the ac singnal frequency increases from 0.01 to 0.59 GHz. The Au/MLM-50/C devices also exhibit a maxima at 0.90 GHz. The frequency based high impedance values means an impedance sufficiently high to inhibit, block or eliminate flow of RF-induced current at a target frequency range(s) [17]. The high impedance value of the Au/MLM-50/C devices compared to that Au/MLM-0/C is attributed to the formation of Li_2O [6] at the ultrathin interface between the stacked layers.

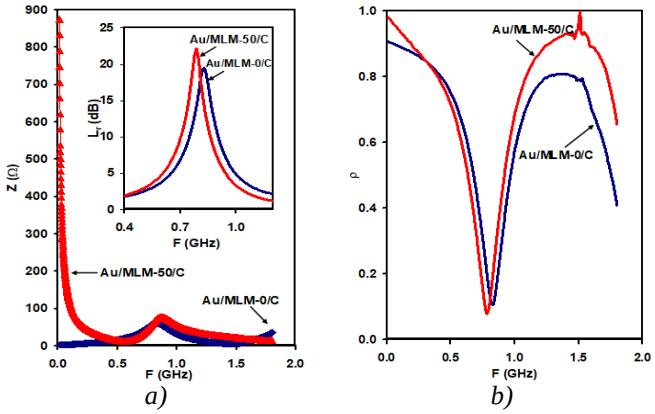

Fig. 4. (a) the impedance and (b) the magnitude of the reflection coefficient spectra for the Au/MLM-0/C and Au/MLM-50/C devices. The inset of (a) shows the return loss spectra.

Fig. 4 (b) illustrates the magnitude of the reflection coefficient (ρ) spectra. ρ is evaluated from the relation, $\rho=(Z_{device}-Z_{source})/(Z_{device}+Z_{source})$ [16]. For a good match between sources and device small values of ρ are required. It should exhibit zero value for perfect matches. However, as such condition is not easily achievable, optimizing a return loss parameter ($L_r=20\log(\frac{1}{\rho})$ [16]) of ~20 dB should be sufficient and acceptable for employing devices for waves trapping issues as microwave resonators. As Fig. 4 (b) and the inset of Fig. 4 (a) illustrates one may obtain a notch frequency of 0.84 and 0.80 GHz accompanied with highest return loss at these

critical frequencies for the Au/MLM-0/C and Au/MLM-50/C devices, respectively. With these features both of the devices appears to be promising for use as low/high passes filters. The insertion of Li slabs between layers of MoO_3 highly improved the return loss values and make the device achieves the commercially accepted values of L_r. The features of the Au/MLM/-50/C devices are comparable to those previously reported for two stacked layers of M_OO_3 sandwiched with indium slabs of thicknesses of 200 nm. This device displayed low pass filter characteristics below 0.30 GHz and high pass characteristics in the frequency domain of 0.35-1.50 GHz [18].

4. Conclusions

In the current study, we have shown that insertion of Li slabs of thicknesses of 50 nm between layers of MoO_3 could significantly alter the morphology through forming rod-like grains without altering the amorphous nature of the films. Electrically, while the presence of Li engineered the negative capacitance effect and changed the resonance-antiresonance peaks positions, it also improved the rectifying properties of the device through increasing the reverse/forward current ratios. The Li nanosheets also changed the high/low impedance status and improved both of the magnitudes of the reflection coefficient and return loss values. The features of the device in the presence of Li layers seem to be more appropriate for application which require control of ac signal propagation as wave traps or microwave resonators and as noise reducers.

Acknowledgments

This work was funded by the University of Jeddah, Saudi Arabia, under grant No. ((UJ-02-092-DR). The authors, therefore, acknowledge with thanks the University technical and financial support.

References

[1] Z. Wang, X. Zhu, Sh. Zuo, M. Chen, C. Zhang, Ch. Wang, X. Ren, Zh. Yang, Zh. Liu, X. Xu, Q. Chang, Sh. Yang, F. Meng, Zh. Liu, N. Yuan, J. Ding, Sh. Liu, D. Yang, Advanced Functional Materials, 1908298 (2019).
[2] R. Kumar, N. Goel, M. Kumar, In 2019 9th Annual Information Technology, Electromechanical Engineering and Microelectronics Conference (IEMECON), pp. 94, IEEE, 2019.
[3] D. Kalaev, A. Rothschild, I. Riess. RSC Advances 7, 38059 (2017).
[4] W. Yang, J. Xiao, Y. Ma, Sh. Cui, P. Zhang, P. Zhai, L. Meng et al., Advanced Energy Materials **9**, 1803137 (2019).
[5] R. Zhang, M. Wu, X. Fan, H. Jiang, T. Zhao, Journal of Power Sources **436,** 226840 (2019).
[6] S. E. Al Garni, A. F. Qasrawi, Physica E Low-dimensional Systems and Nanostructures **114,** 113569 (2019).
[7] H. Shi, R. Asahi, C. Stampfl, Physical Review B **75**, 205125 (2007).
[8] A. Arvind, A. Sarkar, V. K. Shrikhande, A. K. Tyagi, G. P. Kothiyal, Journal of Physics and Chemistry of Solids **69**, 2622 (2008).
[9] S. M. Sze, K. K. Ng. Physics of semiconductor devices, John wiley & sons, 2006.
[10] G. Martinez, C. V. Ramana, Advanced Engineering Materials **19**, 1700354 (2017).
[11] K. K. Bharathi, M. Noor-A-Alam, R. S. Vemuri, C. V. Ramana, RSC Advances **2**, 941 (2012).
[12] S. E. Al Garni, Chalcogenide Letters **14**, 545 (2017).
[13] S. E. Al Garni, A. F. Qasrawi, Chalcogenide Letters **15**, 605 (2018).
[14] R. Jana, J. Datta, S. Sil, A. Dey, B. Pal, A. Biswas, P. Pratim Ray, Materials Research

Express **6**, 1050d1 (2019).
[15] N. M. Khusayfan, A. F. Qasrawi, H. K. Khanfar, Materials Research Express **5**, 026303 (2018).
[16] D. M. Pozar, Microwave engineering. John Wiley & Sons, 2009.
[17] E. Atalar, J. Allen, P. Bottomley, W. Eldelstein, P. V. Karmarkar, MRI-safe high impedance lead systems, U.S. Patent 8,055,351, issued November 8, 2011.
[18] H. K. Khanfar, A. Qasrawi, M. Daraghmeh, M. Abusaa, Microwave and Optical Technology Letters **61**, 2866 (2019).